Available online at www.sciencedirect.com
ScienceDirect
Computerized Medical Imaging and Graphics 30 (2006) 299–313
Computerized Medical Imaging and Graphics
www.elsevier.com/locate/compmedimag

# Automatic segmentation and recognition of anatomical lung structures from high-resolution chest CT images

Xiangrong Zhou [a,*], Tatsuro Hayashi [a], Takeshi Hara [a], Hiroshi Fujita [a], Ryujiro Yokoyama [b], Takuji Kiryu [b], Hiroaki Hoshi [b]

[a] *Department of Intelligent Image Information, Division of Regeneration and Advanced Medical Sciences, Graduate School of Medicine, Gifu University, Yanagito 1-1, Gifu 501-1194, Japan*
[b] *Department of Radiology, Gifu University School of Medicine, Gifu University Hospital, Yanagito 1-1, Gifu 501-1194, Japan*

Received 17 July 2005; received in revised form 21 April 2006; accepted 6 June 2006

**Abstract**

This paper describes a fully automated segmentation and recognition scheme, which is designed to recognize lung anatomical structures in the human chest by segmenting the different chest internal organ and tissue regions sequentially from high-resolution chest CT images. A sequential region-splitting process is used to segment lungs, airway of bronchus, lung lobes and fissures based on the anatomical structures and statistical intensity distributions in CT images. The performance of our scheme is evaluated by segmenting lung structures from high-resolution multi-slice chest CT images from 44 patients; the validity of our method was proved by preliminary experimental results.


*Keywords:* Multi-slice CT image; Three-dimensional image processing; Image segmentation; Lung-structure recognition

## 1. Introduction

Due to the development of multi-slice computer tomography (CT) technology, a modern CT scanner [1,2] can now generate a large number (500–1000) of slices for each patient's CT image scan, covering a large volume of the human body within a short time. Based on this high performance, radiologists can easily photograph the whole human chest, abdomen, or torso with high spatial resolution in a one-time CT scan. Using such high-resolution CT images, observation of complicated anatomical structures in the human body and discovery of small abnormal regions in different organs has become possible. However, CT image interpretations (viewing 500–1000 slices of CT images manually in front of a screen or films for each patient) require a lot of time and energy. Therefore, computer-aided diagnosis (CAD) systems that can support CT image interpretations are strongly anticipated.

The typical requirements for a CAD system can be simply described as "capacity to detect any suspicious regions automatically and show them to a doctor for judgment". Two basic functions (abnormality detection and visualization of CT images) are necessary for a CAD system. In order to realize such functions, a pre-segmentation of the principal human organ regions and recognition of human structures from CT images are always necessary. In the case of chest CT imaging, the lung is the principal region and the lung structure constructed by lung vessels, bronchus, and lung fissures is an important reference for lung cancer, pneumonia and diffuse lung diseases decisions in clinical diagnosis. Recognition of the lung structure is the most basic and indispensable aspect of successful CAD, and definitively influences the efficiency of the overall CAD system. Many research works [3–9] focusing on segmenting a special target region such as the lung, bronchus, vessels, and so on from chest CT images have been reported, few of them have been found to provide global recognition of anatomical structures of human lungs based on high-resolution CT images.

This paper describes a fully automated segmentation scheme for lung-structure recognition based on high-resolution multi-slice CT images. Instead of developing several independent algorithms corresponding to different organ region extractions, our research attempts to recognize the human structures by segmenting the different organ regions simultaneously, based on normal anatomical structure of the human chest and sta-

* Corresponding author. Tel.: +81 58 230 6510; fax: +81 58 230 6514.
*E-mail address:* zxr@fjt.info.gifu-u.ac.jp (X. Zhou).

0895-6111/$ – see front matter © 2006 Elsevier Ltd. All rights reserved.
doi:10.1016/j.compmedimag.2006.06.002

tistical intensity distributions on high-resolution CT images, which contain sufficient and precise three-dimensional (3-D) information on the human chest. The segmentation process has been designed as a recursion of the region-splitting process to identify different organ and tissue regions sequentially, based on a pre-defined order, which is decided based on the spatial and density relations of the those organ regions within the lung structure. Instead of using fixed parameters such as density threshold values for region segmentations, our method attempts to make dynamic parameter optimizations to enhance the compatibility and robustness of CAD system for different CT images. Further, a portion of our processing procedures is designed following a basic policy of "extraction → validation → correction" to enhance the reliability of segmentation results.

This paper is organized as follows. Section 2 simply describes the anatomical structure of the lung region on CT images and shows the concrete goal of lung-structure recognition in our scheme. Section 3 presents the whole policy of our lung-structure recognition method and describes each part of our method in detail. We show our experimental results and give some performance evaluations of our method in Section 4 and provide a summary of this research in Section 5.

## 2. Lung structure

The lung, the site of gas exchange, is filled with air that has a low density (about −1000 HU) on CT images. In addition to air, pulmonary vessels and bronchi are the principal constituents of the lung regions.

Lung regions include the left and right lungs. The left lung is further separated into two lung lobes (upper lobe and lower lobe) by an oblique fissure. The right lung is separated into three lung lobes (upper lobe, middle lobe, and lower lobe) by oblique and horizontal fissures.

The geometry of the bronchial airways in the human chest can be approximately described as a binary tree structure. The trachea (the root of the airway tree) divides into two main branches (left primary bronchi and right primary bronchi), which enter into the right and left lungs. The primary bronchi further divide into five (two left, three right) lobar bronchi that enter each lung lobe, respectively. The lobar bronchi divide repetitively and generate 8–10 segmental bronchi trees in each lung region.

The pulmonary artery and veins are also distributed in a tree structure like that of the bronchial airway in the lung regions. The branch of the pulmonary artery always runs parallel to the bronchi.

Based on the above anatomical knowledge, the goals of our lung-structure recognition scheme can be simply defined as (l) segmenting and dividing the regions over the whole lung into five lung lobes; (2) segmenting the bronchus and recognizing its anatomical tree structure; (3) extracting and dividing pulmonary vessels on a lobe-by-lobe basis; and (4) extracting each inter-lobe fissure – that is, any that are observed to exist on CT images – and refining the lung lobe regions based on the fissure segmentation results.

## 3. Method and materials

Multi-slice chest CT images from 44 patients, generated by 2 kinds of multi-slice CT scanners (in 10 cases, by Aquilion of the Toshiba Medical System; in 34 cases by LightSpeed Ultra of the GE Medical System), are applied as the input data of our scheme. Each patient was imaged by a common protocol (l20 kV/Auto mA, helical pitch: 1.35/1) without any contrast enhancement, and the images were created using a normal reconstruction kernel and stored in Digital Imaging and Communications in Medicine (DICOM) format [10]. After DICOM format decoding, each patient case of CT images was expressed as a $512 \times 512 \times 400$–$633$ matrix that covered the entire human chest region with an isotropic spatial resolution about 0.63–0.74 mm and 12-bit density resolution. The output of our scheme is a 3-D image in which each voxel has been attached with a pre-defined label that can be used to refer to the lung structure shown in the previous section.

The basic idea of our method can be simply described as "using the air-filled region inside the human chest to estimate the range of various lung regions and using airway tree of the bronchi to recognize anatomy structures in the lungs". Our scheme tries to recognize the details of these human structures gradually as shown in Fig. 1. The process consists of five main steps: (l) initial region segmentation of chest CT images, (2) extraction of the trachea and bronchi and recognizing the branches of the bronchi tree, (3) extraction of the lung regions and separation of the left and right lung, (4) extraction of pulmonary vessels, and (5) division of the lung regions into five lung lobes and extraction of the inter-lobe fissures. Each of these steps is described in detail in the next section.

### 3.1. Initial region segmentation of chest CT images

The goal of this step is to separate human body regions from background and make an initial classification that divides the human body region into three components: fat, other tissues (including bone, organ, vessels, and so on) and air-filled regions, as shown in Fig. 2. We use a gray-level thresholding method to identify the regions based on their respective density distributions. Instead of using fixed threshold values to segment target regions, our process uses a histogram analysis method that can determine the optimal threshold value just for the current CT image automatically. The details of this step are as follows.

#### 3.1.1. Preprocessing of CT image

We extract the CT image data slice-by-slice from DICOM format files and arrange them into a 3-D data array based on the information inside the DICOM heads. This 3-D data array is regarded as the original CT image (Fig. 2(a)); it has nearly isotropic spatial resolution in 3-D.

#### 3.1.2. Threshold value selection

The next step is to decide the optimal threshold value for segmenting human tissues from the background that is almost filled by air. We assume that the total region of a CT image consists

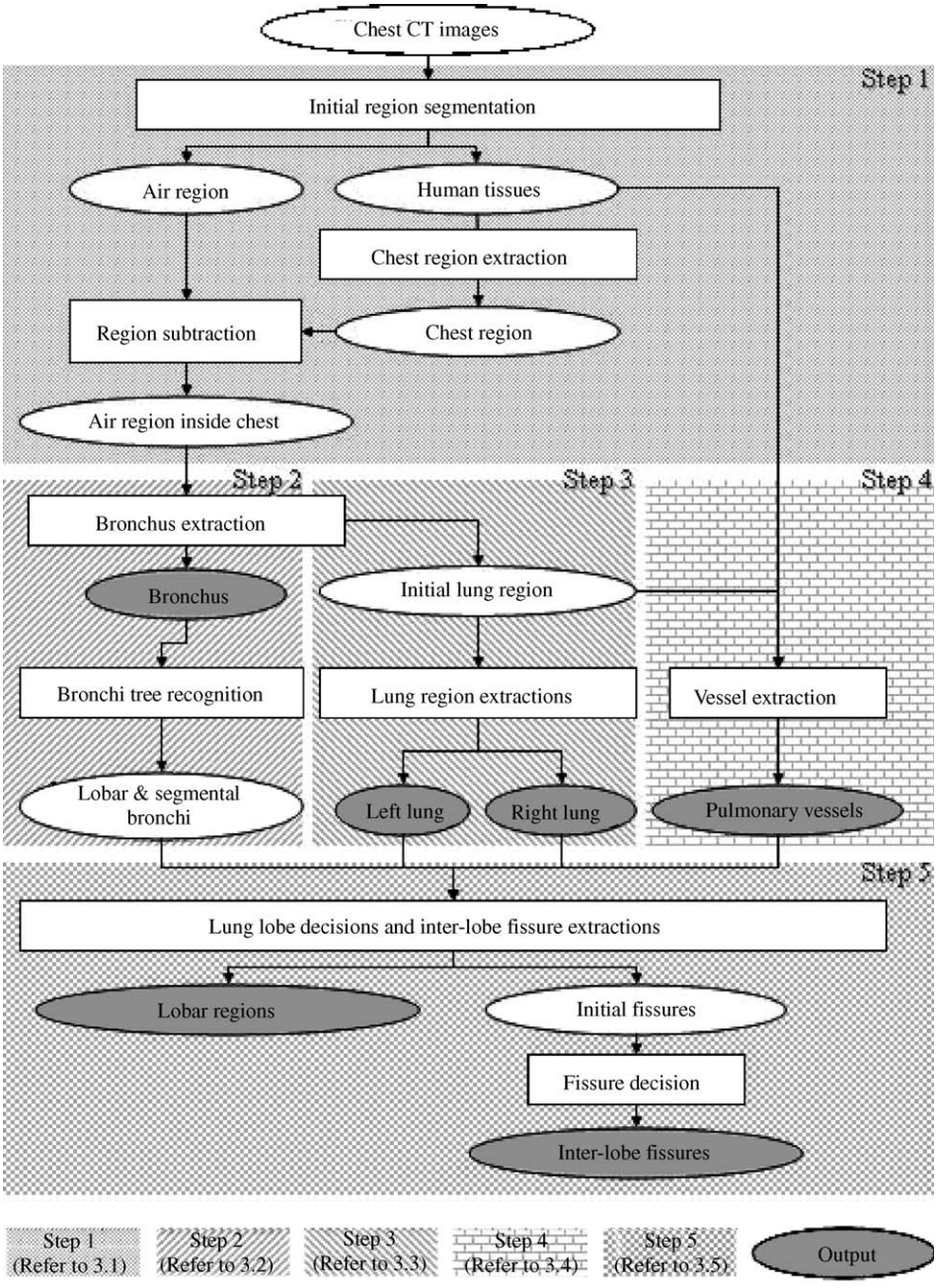


Fig. 1. Processing flow of lung-structure recognition scheme.

of only two components: air regions and human tissue regions with different density distributions. We measure the degree of separation between those two density distributions on a gray-level histogram using a discriminant analysis [11], and select the gray level ($T_1$ in Fig. 3) that has the maximum value of separation degree as the optimal threshold value for segmenting human tissues, as distinct from air regions (refer to Fig. 3). Due to the relation of density distributions among different human tissues shown in Fig. 4, the fat can be separated from the other tissues using the CT value of water, which is about 0 (HU). We use a process to select the optimal gray level ($T_2$ in Fig. 3) by searching for the zero-cross point of differential values on the histogram – that is, the point nearest to 0 (HU) – and use it to identify fat regions (Fig. 3).

### 3.1.3. Gray-level thresholding

Using the selected threshold values $T_1$ and $T_2$, we separate human tissues from background as follows:

| | |
|---|---|
| If (gray level <= $T_1$) | VoxelLabel = Air |
| Else if ($T_1$<gray level < $T_2$) | VoxelLabel = Fat |
| Else | VoxelLabel = Other tissues of human body |

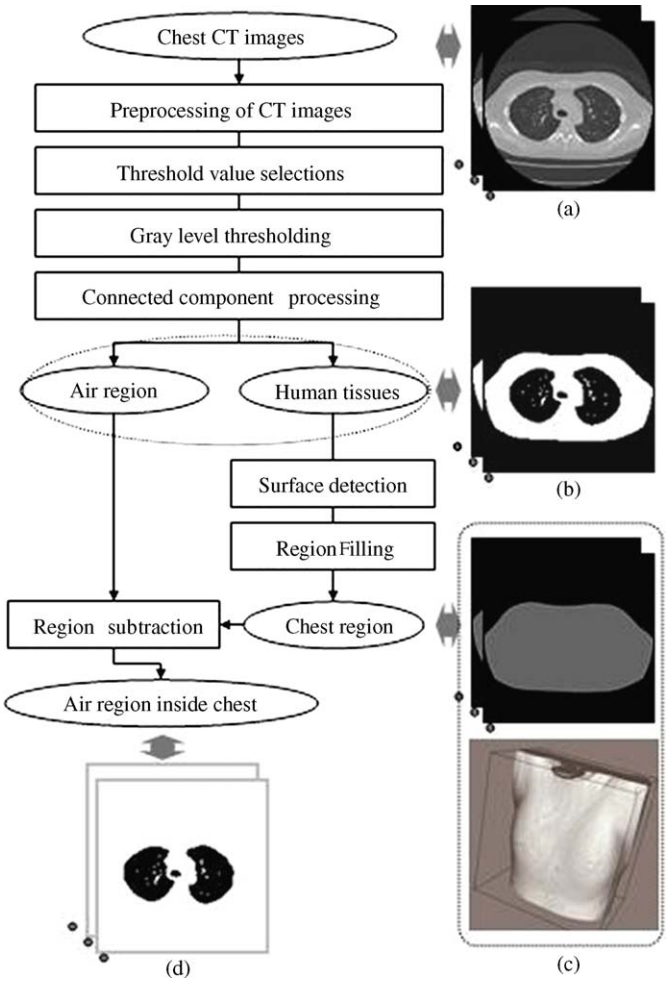


Fig. 2. (a–d) Processing flow of initial region segmentation (step 1 of Fig. 1).

### 3.1.4. Connected component processing

We use the 3-D connectivity analysis to select the connected component (18-neighborhood) with the biggest volume from human tissue regions (gray level $> T_1$) as the real chest region (Fig. 2(b)) and delete the remaining regions.

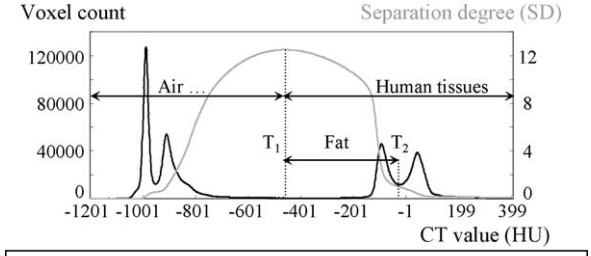


$$SD = \frac{(M_{tissue} - M_{all})^2 \times Vol_{tissue} + (M_{air} - M_{all})^2 \times Vol_{air}}{Var_{tissue} \times Vol_{tissue} + Var_{air} \times Vol_{air}}$$

$M_i$ = Mean of the CT values in region i
$Var_i$ = Variance of the CT values in region i
$Vol_i$ = Volume of region i

Fig. 3. Threshold value selections based on histogram analysis.

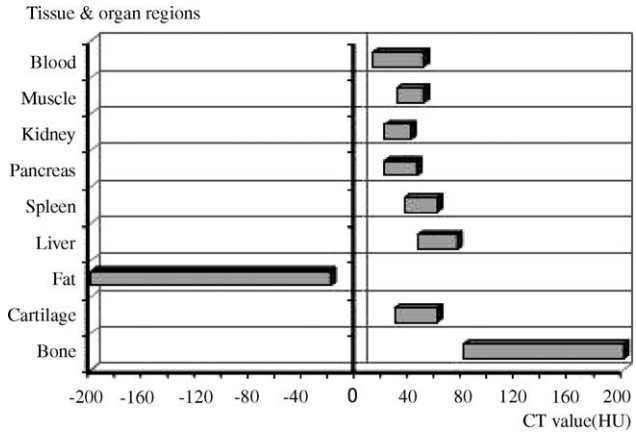


Fig. 4. CT value distributions in different organ and tissue regions.

### 3.1.5. Surface detection and region filling

We extract the outline of the human chest using a 2-D border following method that traces the external borderline between human tissue region and air region slice-by-slice. Then, we simply use the whole region circumscribed by the borderline, regarding it as the chest region (Fig. 2(c)).

### 3.1.6. Region subtraction

We identify the air regions inside the human chest by subtracting the air region (black region in Fig. 2(b)) from the chest region (gray region in Fig. 2(c)) and finally output the latter (Fig. 2(d)).

## 3.2. Trachea and bronchus extraction and bronchial tree recognition

The trachea and bronchus have a tubular structure and are filled with the air, which means we can identify the tracheal and bronchial region by extracting the airway tree from the air region inside the human chest (output of step 1 in Fig. 1). For extracting the airway tree, many techniques have been developed [3–5], and 3-D region growing method has been proven a very effective one, though the extraction accuracy using 3-D region growing is very sensitive to the threshold value that is used for controlling the region expansion. Mori et al. proposed a method to determine the optimal threshold [5].

This method is to expand the airway region gradually by increasing the threshold value until the segmented region leaks into the lung, and to regard the threshold value just prior to the region leak as the optimal one. The judgment of region leak is based simply on observing whether the volume increase of the segmented airway region goes beyond a limitation (threshold value) during the repetition of the 3-D region growing process (refer to Fig. 5). This method is very effective for some ideal cases such as that shown in Fig. 5(a). However, due to the influence of noise, motion artifacts or disease, the airway wall is collapsed or discontinuous at some branches shown on CT images. Those discontinuities in the bronchus wall cause the airway region to merge into the lung slowly and prematurely during the

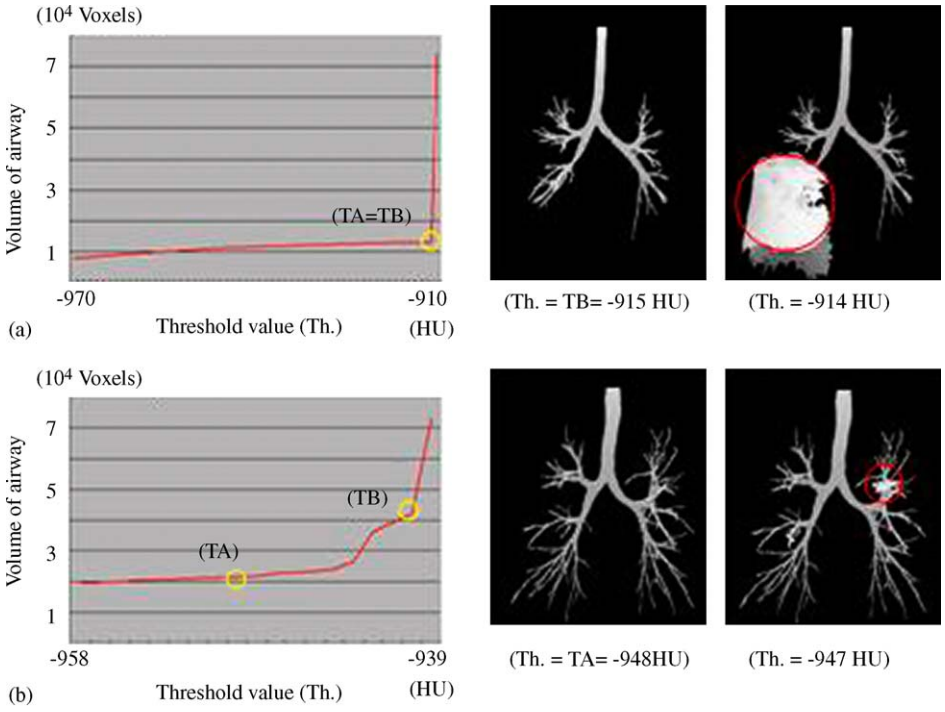


Fig. 5. Threshold value decision of 3-D region growing process. (a) Case 1: Optimum Th. value is decided correctly. (b) Case 2: Optimum Th. value is decided incorrectly. TA: Th. value of manual decision. TB: Th. value of automated decision. (○) Leak region.

region growing process, and result in airway extraction failure (Fig. 5(b)).

We propose a new method for airway extraction and recognition. This method, like Mori's, also uses 3-D region growing as the basic process. The difference between our method and that of Mori is that: (l) we validate the regions by reference to the structure of airway trees (common anatomical knowledge), which information is used as feedback to avoid or eliminate the influence of leak during the airway region extraction. (2) Instead of using one threshold value for extracting the total airway region, we analyze and segment the airway region based on a branch-by-branch basis, and decide the optimum threshold value for each branch individually and specifically. The processing flow of our method (shown in Fig. 6) includes two main steps. We describe each of these steps in detail as follows.

*3.2.1. Step 1: Extracting the initial airway region*

Based on the results of the initial region segmentation process, we select the air region inside the human body (refer to Fig. 2(d)) in the first slice (nearest to the head) on the 3-D chest CT image as the seed points of the airway region. Then we estimate the optimum threshold value using Mori's method [5], and use it to extract the airway region by a branch-based 3-D region growing method [12]. Compared with the region growing method of Mori [5], this method can recognize the branch points during the region growing process and output the airway region into a binary tree structure by attaching to each branch a unique label. We show each labeled branch in the airway tree in a different color in Fig. 6(a and b). By matching this labeled airway tree with the normal anatomical bronchus tree structure, we can identify the parent branch of the leak region, which always has a lot of offshoots or sub-trees. In our process, we use the following rule to detect and delete the leak regions:

```
For I = Root node to End nodes of airway tree
    {If (NumofOffshoots from I node > 2* AnatomyNum from I node)
        {Mark I as the end node of airway tree
         Cut off the airway tree in node I and throw off the child branches of I}
     Else If ( I> MaxDepth of airway tree)  /* we set MaxDepth = 8 here */
         Cut off the airway tree in node I and throw off the child branches of I}
```

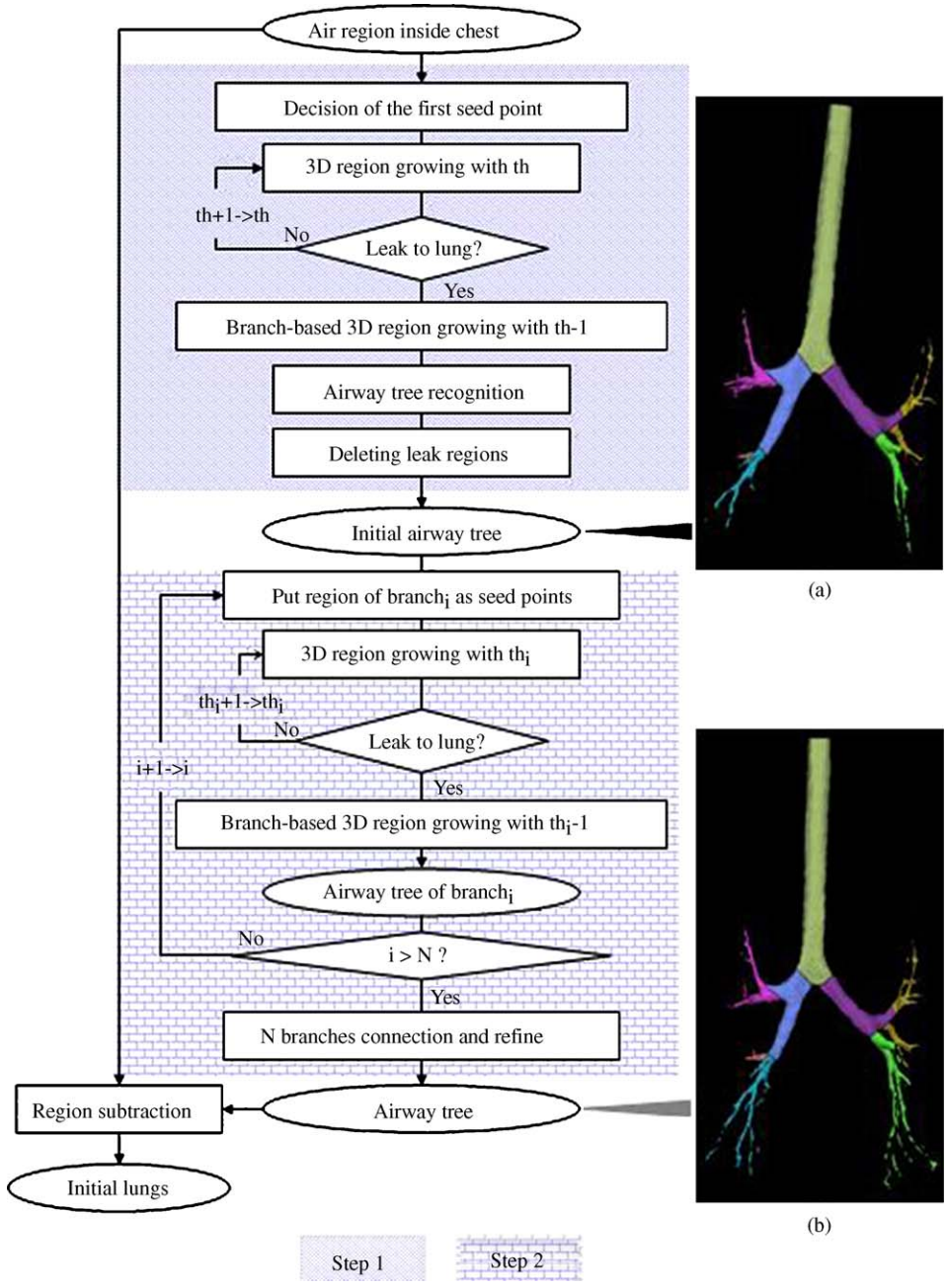


Fig. 6. (a and b) Processing flow of airway tree extraction and recognition (step 2 of Fig. 1).

Next, we output the refined airway tree as the initial airway region, as shown in Fig. 6(a).

### 3.2.2. *Step 2: Refine the airway region by branch-by-branch basis processing*

Due to the influence of leak regions in some sub-branches, the region growing process based on single threshold value in step 1 has a limited performance for peripheral branch extractions. Here, we separate the airway region into branch units based on anatomical bronchus tree structure firstly, and then, each of the branch units is regarded as the root of a sub-tree of bronchus. The region growing method as described in step 1 is used again to refine each sub-tree and extract peripheral branches which are not indicated in initial airway region (Fig. 6(a)).

Finally, we just retain the branch regions within the 12th node in depth of the airway tree structure as reliable branches and output it as shown in Fig. 6(b). As another result, we remove the airway of the bronchus from the air region inside chest, and regard the remaining air regions as the initial lung region for the next processing step.

## 3.3. *Lung region extraction*

Many investigations for lung region segmentation from CT images have been reported [6–8]. Almost all of those reports use

the air region inside the human chest to estimate the shape of lung regions. However, how to separate the connection between the mediastinum and the lung region without changing the shape of the lung surface is a problem that has not yet been completely solved. We proposed a processing procedure (shown in Fig. 7) that attempts to extract the lung region and preserve the shape of lung surface as precisely as possible. As the first step, we separate the initial lung region (output of Section 3.2) into left lung and right lung using the following algorithm.

```
Remove the small connected components by a volume thresholding
Perform a 3-D hole-filling for each connected component region
FlagOfSeparation=0
If (Number of connected components =1){   // left and right lung are fused together//
    FlagOfSeparation = 1
    Repeat 3-D region shrinking until (Number of connected component>1)}
Select the first and second connected component from the larger volume order
Identify the selected 2 regions into left and right lung by comparing their center location
If (FlagOfSeparation = 1)
 {Deciding the junction lines of left and right lung region using 3-D watershed method
  Separating left and right lung region based on junction lines}
```

Next, we extract the surfaces of the left and right lung regions by a 3-D border following method and divide the respective lung surfaces into facies diaphragmatica, facies costalis, and facies medialis, as shown in Fig. 7(a). The facies diaphragmatica are the lung surfaces that lie immediately against the diaphragm and the facies costalis are the lung surfaces that lie immediately adjacent to the ribs and intercostals space of the thoracic wall. The facies medialis are the lung surfaces that lie against the mediastinum anteriorly and the vertebral column posteriorly and contain the comma-shaped hilum of the lung through which structures, such as blood vessels and bronchus, enter and leave. Our scheme uses the curvature and normal vector in each voxel on the lung surfaces for the lung surface division process by the following seven steps.

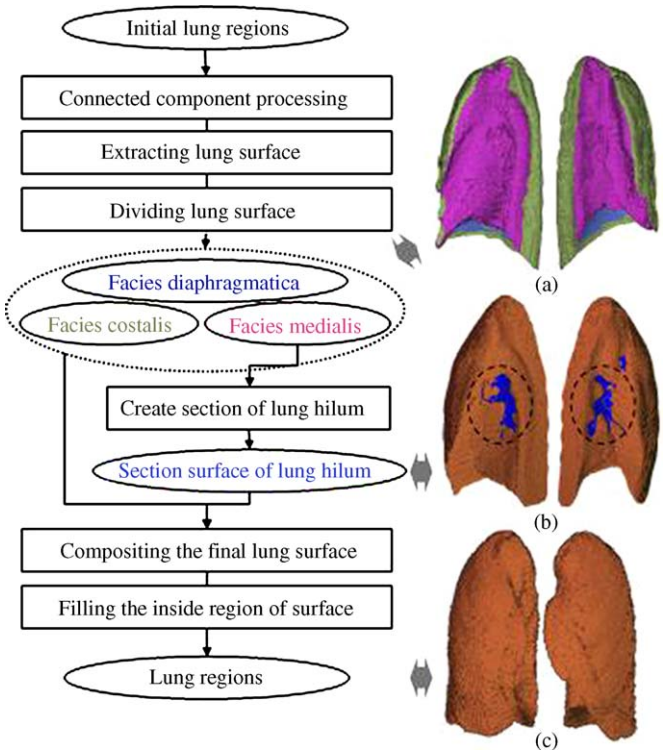


Fig. 7. (a–c) Processing flow of lung region extraction (step 3 of Fig. 1).

(1) The local lung surface for each voxel was modeled with a second-degree polynomial on a $5 \times 5$ neighborhood and was optimized using the least squares method.
(2) The normal vector **V**, mean curvature **H**, and Gaussian curvature **K** for each voxel of lung surfaces were calculated using the estimated surface.
(3) The candidate voxel **P** of facies diaphragmatica was restricted to the condition such that $[-\Pi/4 <$ direction of **V** on **P** $< +\Pi/4]$ where the longitudinal axis of the body was taken as zero radian.
(4) The largest connected component of the candidates on the left/right lung surface was determined to be the initial left/right facies diaphragmatica and refined by a region growing method.
(5) The candidate voxel **P** of facies costalis was restricted to the condition such that [**H** on **P** $< 0$] and [**K** on **P** $> 0$] and [3-D distance from **P** to the bone $< 3$ mm].
(6) The largest connected component of the rest lung surfaces on the left/right lung surface was determined to be the candidate of facies medialis.

(7) A Voronoi division based on the 3-D distances to the candidates of facies medialis and facies costalis was used to identify the finial surfaces of facies medialis and facies costalis on the left/right lung surface [13].

In order to close the lung hilum, we create an approximate surface by smoothing the facies medialis using a binary morphological operator, and then we identify the position of the lung hilum and create a section surface of lung hilum (Fig. 7(b)) for the right and left lung, respectively, by use of the following algorithms [13].

Section of Lung hilum = Biggest partial surface in S
whose distance to X bigger than T
$S = (X + B^s) - B$
X : Facies medialis
B : Structure element (a ball region with radius = 15 voxel)
+ - : Minkowski operators
T : A threshold value (set as 2, by experience)

Using this method, we can just close the lung hilum and preserve the original lung shape (excepting the hilum) as precisely as possible [13]. Finally, we fill the inside regions of closed lung surfaces and output this area as lung regions (Fig. 7(c)).

### 3.4. Pulmonary vessel extraction

The algorithm used for pulmonary vessel extraction is similar to the bronchus region extraction method described in Section 3.2. We first select the human muscle regions inside the lung region as the seed points for 3-D region growing (Fig. 1). Then we use a processing flow (similar to the airway extraction in Fig. 6) to extract the pulmonary vessels by two steps. First, we extract the initial pulmonary vessels by 3-D region growing based on a single threshold value which is decided automatically using a similar process as shown in Fig. 6(step l), then, we divide the pulmonary vessels into tree structures and refine each branch of the pulmonary vessel trees based on a branch-by-branch analysis. This process is similar to Fig. 6(step 2). Lastly, we separate a part of initial pulmonary vessels near to the surface of airway of bronchus and regard it as the bronchial wall by the following algorithm.

For each voxel i of initial pulmonary vessels {
{$D_i$ = Minimum distance to the surface of airway of bronchus
If ($D_i$ < th ) $D_i$ -> bronchial wall region // th: a threshold value //}

Refine the bronchial wall region using 3-D connected component processing
Pulmonary vessels region = initial pulmonary vessels - bronchial wall region

### 3.5. Lung lobe decisions and inter-lobe fissure extractions

Inter-lobe fissures, thin membranes with a thickness of about 1–2 mm, separate the lung region into different lung lobes. The fissures are not truly visible on each CT image; they appear as a thin surface pattern with a weak density. Because of the image noise, motion artifacts of breathing, and occasional presence of disease, in many cases (about 70% of patients), the inter-lobe fissures cannot be observed completely on CT images [14,15]. Due to this fact, it is very difficult for a CAD system to extract the inter-lobe fissure automatically solely on the basis of density on CT images. Here, we propose an anatomy-based method to extract lung lobar regions and identify inter-lobe fissures automatically. The basic idea of this method is to recognize the lobar bronchus and vessels and use those structures to divide the whole of the lung regions into five lung lobar regions first; use the boundary between the different lung lobes to estimate the inter-lobe fissure locations; and then make a precise extraction of real fissures by detecting the edges around the estimated fissure locations. The processing flow of this method includes three main steps, as shown in Fig. 8. The details of each step are as follows.

#### 3.5.1. Lobar vessel classifications

We classify the cumulative lung vessels into five lobar groups (Fig. 8(d)) based on the bronchial tree structure recognized before. By checking the connection of lung vessels to each lobar bronchial wall, we can determine the representative voxels of vessel regions belonging to each lobe region, and determine the other voxels by searching the minimum distance to each lobar representative voxel via the vessel tree. The details of this algorithm are shown below.

```
Get each lobar bronchus from the bronchial tree
For I= 1 to 5 { //   I : lobar identification number
 If voxel belongs to lung vessels and connects with I lobar bronchi wall
        Regard this voxel as a seed point of lobe I}
For each voxel of lung vessels
 {Get the 3-D distances between current voxel and each seed point via lung vessels
 Search for the nearest seed point A from current voxel
 Attach current voxel with the same lobe identification number of A }
```

*3.5.2. Dividing lung regions into five lung lobes*

We have classified the bronchus and vessels into five lobar groups by the above steps. Based on that information, we divide the whole lung into five lobar regions using a Voronoi division algorithm. More specifically, we firstly set each lobar vessel and bronchus group as the "skeleton" of the corresponding lung lobar region, and then measure the 3-D distances from the "skeleton" of each lobar region to each voxel of the lung region using the 3-D Euclidean distance transformation method [16]. Finally, we classify each voxel of the lung region into a specific lung lobe whose "skeleton" is nearest to it.

*3.5.3. Inter-lobe fissure extractions*

Using the extraction results of the five lobar regions, we define the boundary surface between the different lobar regions as the initial locations of inter-lobe fissures (Fig. 8(f)).

Due to the accuracy of lung vessel and bronchus extractions, the positioning of initial fissures may, in many cases, suffer a small shift in comparison to the real fissures. Here, we limit the scope around the initial fissures and do a further extraction of fissures by detecting the surface pattern based on density distribution on the original CT images. More specifically, we expand the initial fissures using a 3-D morphologic filter with a ball structure and generate a slab region with a thickness of 10 mm around the initial fissures; use an 18-neighborhood Laplacian filter (mask size: 1.5 mm) to enhance the original CT image; and then extract the edge elements based on zero-crossing detection within the generated slab regions. Lastly, we select a connected component which has the biggest projection area on the surface of a corresponding initial fissure from of edge elements and adjust it to a smooth surface pattern by a morphological operator. We regard these smooth surface patterns as the final results of inter-lobe fissures (Fig. 8(g)). At last, we use the inter-lobe fissures to re-separate lung regions into five lobar regions again by a 3-D connected components processing (Fig. 8(h)). If the lung region re-separation is not successful, we decide that the inter-lobe fissures are incomplete and regard the lung lobar regions decided by the initial lung fissures as the final results.

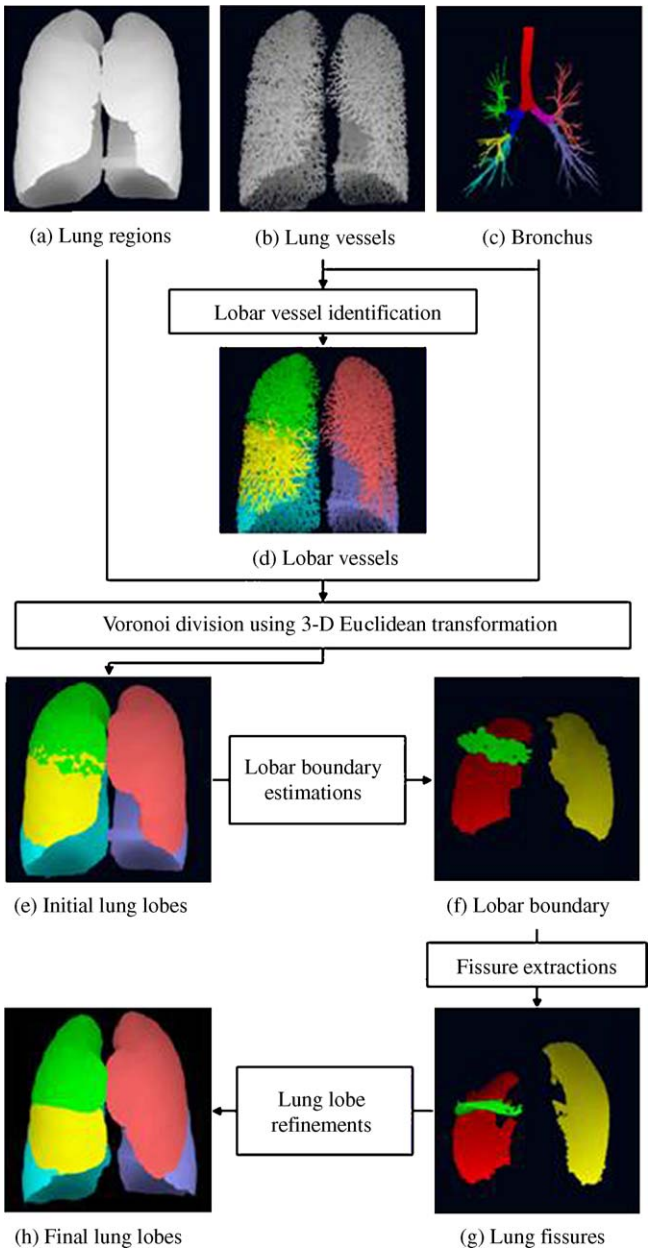


Fig. 8. (a–h) Processing flow of lung lobe and fissure extractions (step 5 of Fig. 1).

## 4. Results and discussion

We assessed the performance of our automated human chest structure recognition method using chest multi-slice CT images from 44 patients. Excluding the three cases which had serious

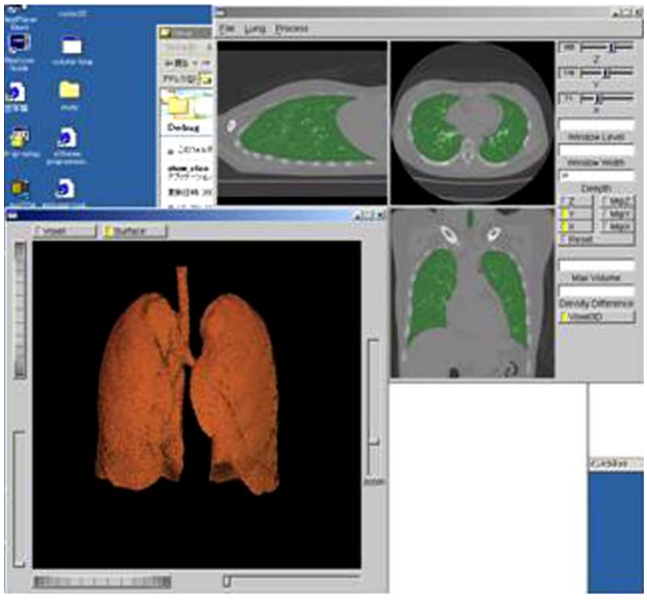

Fig. 9. A user interface for visual evaluation on accuracy of the segmentation results (green) in CT images. "For interpretation of the references to color in this figure legend, the reader is referred to the web version of the article".

pneumonia or pulmonary emphysema, the remaining patients had almost normal lung structures that could be confirmed by physicians from CT images.

Human tracings of target regions were used as the gold standard of evaluation of region extraction accuracy of a CAD system from a CT image. However, in the case of a high-resolution CT image that includes 400–633 slices, it is very time consuming to draw the tracings slice-by-slice and difficult to maintain high accuracy of the human tracings in 3-D. Here, we developed a special user interface for accuracy evaluation to reduce this burden [17]. This interface can show the segmentation regions semi-transparently on a CT image (Fig. 9). The human expert can use this tool to give an evaluation intuitively and quickly by viewing the segmentation results from 3-direction slice-by-slice and 3-D shape of segmentation regions (Fig. 9). In our experiments, we used this interface to evaluate the accuracy of automatic extraction results of chest, fat, vessel, and lung regions. We selected seven patient cases and made a human sketch of body surface, lung surface and lung fissures as the gold standard (the human sketches were decided by one of the authors (Dr. T. Kiryu) who is a radiologist on chest diagnosis). We made a quantitative evaluation by comparing the segmentation result with the gold standard. Two methods had been mainly used for accuracy evaluation.

(a) Coincidence degree had been used for mass regions evaluation:

$$\text{Coincidence degree} = \frac{\text{A} \cap \text{M}}{\text{A} \cup \text{M}}$$

A: mass region extracted automatically; M: mass region extracted manually.

(b) Average shortest Euclidian distance (ASED) had been used for surface pattern evaluation:

$$\text{ASED} = \frac{\sum_{i \in s1} \text{SED}(i, s2)}{V}$$

$s1$, $s2$: surface patterns; SED($i$, $s2$): the shortest Euclidian distance from pixel $i$ to a surface $s2$; $V$: area (voxel number) of surface $s1$.

Beside of the ASED, we also defined SSED (standard deviation (S.D.) of the shortest Euclidian distance for each pixel in extracted surface to a target surface) and MSED (maximum value of the shortest Euclidian distance for each pixel in extracted surface to a target surface) to measure the coincidence between two surface patterns.

We show a portion of the lung-structure segmentation results (5 successful cases in Fig. 10 and 3 cases of failure in Fig. 11) by displaying the principal sub-structures (airway tree of bronchus, lung vessels, lung lobes, lung fissures) of the lung region in 3-D and 2 representative slices of CT images overlapped by the extracted inter-lobe fissures. Further detailed structures in each result image are shown in different colors for ease of identification.

Our segmentation scheme using a sequential region-splitting process to recognize the different organ and tissue regions sequentially and precisely based on the anatomical structure of the human chest has been proved effective from our experimental results. We confirmed that our method could recognize, correctly and stably, the lung structure from 41 patient cases in which the normal lung structure could be almost identified visually on CT images. For the remaining patient cases (two cases with heave pneumonia, one case with abnormal airway structure), the anatomy lung structure could not be distinguished clearly even by an expert physician. In such cases, our method simply stopped the recognition process and output a warning message. In the following section, we give detailed performance evaluations for each processing step of our scheme.

### 4.1. Initial region classification

We confirmed that our method shown in Fig. 2 could identify the region of air and perform extraction of the human chest accurately and stably for all (44) of the patients. We compared the extracted chest region to the manual sketch for 7 cases and confirmed the coincidence degrees of each case varied from 99.41 to 99.91% (the mean value was 99.57% and standard deviation was 0.35%). Further, we measured the ASED for each voxel on the chest surface to the manual sketch and found the values varied around the mean value of 0.32 mm with a standard deviation of 0.15 mm (Table 1). We verified the density thresholding values (Fig. 12), which were decided automatically for adapting the different patient cases by our method (Fig. 3), and confirmed that the selected threshold value was the optimum one for each patient case. From the above results, we confirmed that our thresholding value selection method is necessary and effective for adapting to differences among inputted CT images.

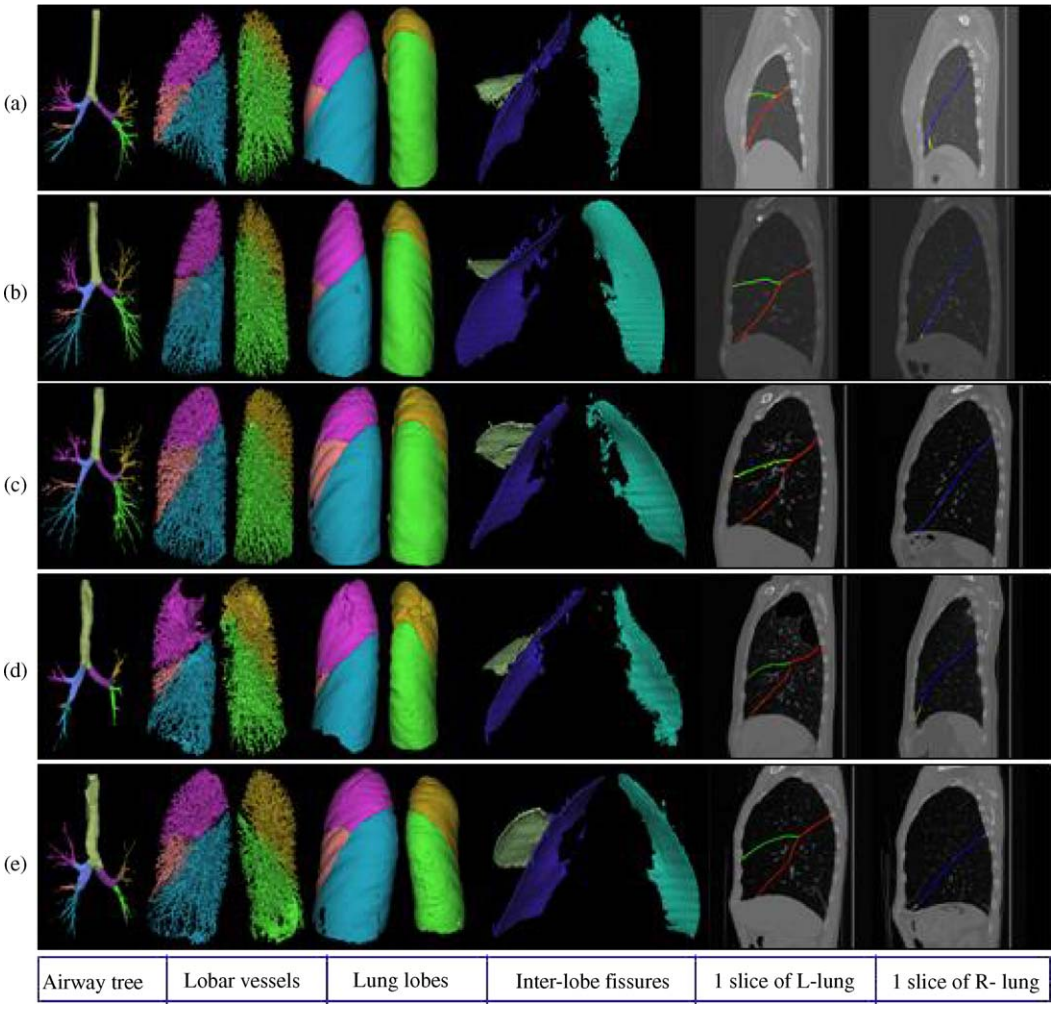


Fig. 10. Segmentation results of lung structures. (a–e) Five patient cases.

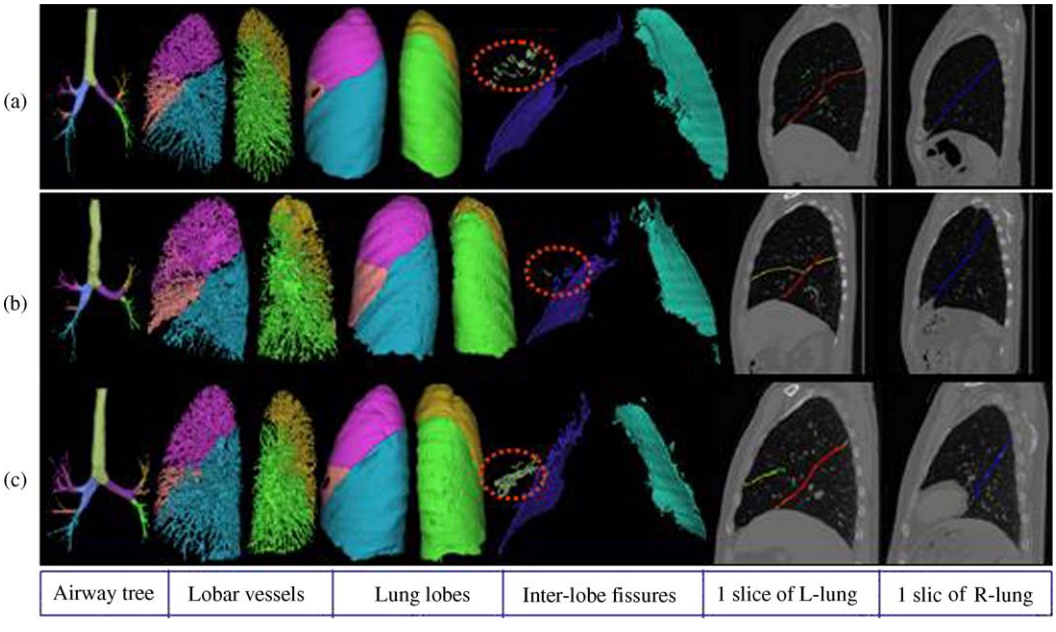


Fig. 11. Segmentation results of lung structures. (a–c) Three patient cases. (◌) Misidentifications due to incomplete fissure in original CT images.

Table 1
The accuracy evaluations for the segmentation results of chest region using manual tracings

| Case no. | Accuracy of the chest region segmentation | | | |
|---|---|---|---|---|
| | $C^*$ (%) | ASED (mm) | SSED (mm) | MSED (mm) |
| 1 | 99.41 | 0.29 | 0.16 | 4.42 |
| 2 | 99.76 | 0.28 | 0.19 | 7.95 |
| 3 | 99.91 | 0.20 | 0.17 | 9.08 |
| 4 | 99.65 | 0.24 | 0.16 | 3.13 |
| 5 | 99.63 | 0.31 | 0.18 | 4.00 |
| 6 | 99.76 | 0.23 | 0.15 | 3.75 |
| 7 | 98.85 | 0.66 | 0.96 | 7.13 |
| Mean | 99.57 | 0.32 | 0.28 | 5.64 |
| S.D. | 0.35 | 0.15 | 0.30 | 2.36 |

$C^*$: Coincidence degree between the segmentation results and the manual tracing.

### 4.2. Airway extraction and airway tree recognition

Our method identified the airway regions successfully for all (44) the patients, and recognized the anatomical tree structure from 98% (43/44) of patients successfully, as shown in Figs. 10 and 11, respectively. The tree structure recognition process failed in one patient case because the airway of this patient had an abnormal tree structure; it differed quite a bit from the standard anatomical structure. We confirmed that the trachea and lobar bronchus were completely extracted and recognized correctly from 43 patients. Due to the limitation of image quality and patient's personality, the situations of segmental branches in CT images were varied largely in different cases. The numbers of segmental bronchi that were extracted in each lobar region are shown in Table 2. About 17.5 branches in the segmental bronchial tree were extracted in each lobar region for each patient. The standard deviation of the extracted segmental branches was about 12. This result showed the approach of our method (extraction → recognition → adjusting) could enhance the flexibility for different cases and was effective to enhance the reliability of extraction results.

### 4.3. Lung region extraction

The basic policy of our method for lung region extraction is to identify the air region within chest and use it to estimate lung surface. We found that this policy was effective for 95% (42/44) patients. In the remaining two patient cases, the lung regions were filled by inflammation that appeared as high-density fibrous regions. Although the air regions inside the lungs were extracted successfully by our method, the information was insufficient to estimate the lung surface precisely. For 42 patient cases, we confirmed that the lung regions from the left and right lung were identified and separated successfully. We evaluated the accuracy of the lung region extraction by calculating ASED, SSED and MSED for each pixel on the lung surface (excepting lung hilum) to the manual sketch using seven patient cases and confirmed the mean value between extracted lung surface to the manual sketch was 0.44 (mm) in case of left lung, and 0.62 (mm) in case of right lung (Table 3). Beside of the left lung region in cases 5 and 6, which a nodule on the lung wall caused a big value of MSED, the maximum distance between extracted lung surface and manual sketch was about 4.5 mm in left lung and 8.9 mm in right lung (Table 3). Using the evaluation tool shown in Fig. 9, we found that our method closed lung hilum successfully and preserved the shape of the other lung surfaces precisely. It can be considered that lung surface dividing and limiting the location of lung hilum for smoothing are necessary for lung region extraction.

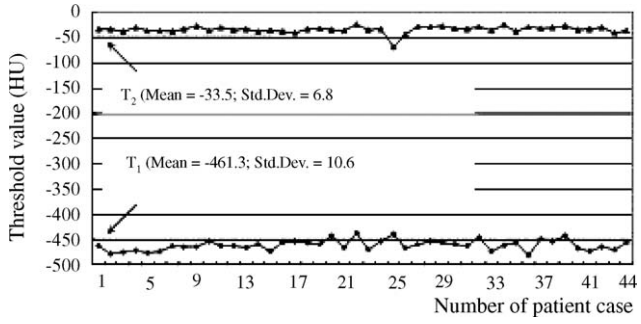


Fig. 12. Threshold values decided automatically for different CT images.

Table 2
The numbers of the extracted segmental bronchi in each lobar region

| 43 cases | Number of bronchus | | | | |
|---|---|---|---|---|---|
| | Right lung | | | Left lung | |
| | Lobus superior | Lobus medius | Lobus inferior | Lobus superior | Lobus inferior |
| Mean | 20.9 | 8.8 | 16.7 | 22.6 | 18.8 |
| S.D. | 11.0 | 10.5 | 7.4 | 18.7 | 12.5 |
| Maximum | 67.0 | 56.0 | 40.0 | 108.0 | 72.0 |
| Minimum | 3.0 | 1.0 | 6.0 | 7.0 | 6.0 |

Table 3
The accuracy evaluations for the segmentation results of lung region using manual tracings

| Case no. | Accuracy of the lung region segmentations | | | | | |
|---|---|---|---|---|---|---|
| | Right lung | | | Left lung | | |
| | ASED (mm) | SSED (mm) | MSED (mm) | ASED (mm) | SSED (mm) | MSED (mm) |
| 1 | 0.63 | 0.36 | 2.80 | 0.32 | 0.20 | 6.16 |
| 2 | 0.63 | 0.41 | 8.71 | 0.54 | 2.71 | 19.20 |
| 3 | 0.72 | 0.28 | 3.42 | 0.34 | 0.25 | 8.22 |
| 4 | 0.65 | 0.29 | 3.95 | 0.49 | 0.37 | 10.16 |
| 5 | 0.69 | 0.31 | 2.80 | 0.42 | 0.56 | 96.25[a] |
| 6 | 0.38 | 0.20 | 4.10 | 0.51 | 4.18 | 116.76[a] |
| 7 | 0.68 | 0.41 | 5.69 | 0.44 | 0.27 | 6.76 |
| Mean | 0.62 | 0.32 | 4.49 | 0.44 | 1.22 | 10.10 |
| S.D. | 0.11 | 0.07 | 2.10 | 0.08 | 1.58 | 5.32 |

[a] The errors were caused by lung nodules on lung wall.

Table 4
The accuracy evaluations for the segmentation results of lung lobes using manual tracings

| 7 cases | Coincident degree of lobar volume (%) | | | | |
|---|---|---|---|---|---|
| | Right lung | | | Left lung | |
| | Lobus superior | Lobus medius | | Lobus superior | |
| Mean | 98.54 | 97.21 | 98.62 | 98.49 | 98.46 |
| S.D. | 0.69 | 0.87 | 0.67 | 0.30 | 0.50 |
| Maximum | 99.27 | 98.13 | 99.23 | 99.13 | 99.19 |
| Minimum | 97.55 | 96.12 | 97.27 | 98.25 | 97.59 |

Table 6
The accuracy evaluations for the final segmentation results of lung fissures using manual tracings

| 7 cases | ASED (mm) | | |
|---|---|---|---|
| | Right lung | | Left lung |
| | Oblique fissure | Horizontal fissure | Oblique fissure |
| Mean | 0.52 | 0.30 | 0.68 |
| S.D. | 0.23 | 0.08 | 0.29 |
| Maximum | 1.00 | 0.41 | 1.01 |
| Minimum | 0.32 | 0.20 | 0.31 |

### 4.4. Lung vessel extraction

Except in 2 patient cases with pneumonia, the lung vessel regions were identified correctly from the 42 patients (Figs. 10 and 11). However, some lesion regions (lung cancer, inflammations, etc.) were misclassified as a part of the lung vessels. A further validation of vessel extraction results is necessary and should be incorporated into our method in the future.

### 4.5. Lung lobe region extractions

For the 41 patients whose lung regions and airway of bronchus were extracted and recognized correctly, our method divided the left and right lungs into 5 lobar regions successfully (Figs. 10 and 11). In order to test the performance of our method, we tracked inter-lobe fissures slice-by-slice and separated the lung region into five lobar regions manually from seven patient cases whose inter-lobe fissures could be observed clearly and completely on CT images. We compared each automated extraction result of lobar regions with the manual segmentation results by measuring coincidence degree. The coincidence degree for each lobar region was shown in Table 4. We confirmed that the results extracted automatically and the manual results were extremely consistent with a high coincidence degree about 98%. This indicates that our approach—"lung lobar region identification based on anatomy structure of the airway tree"—was successful. We measured the ASED from approximated lobar boundaries to the manual fissures, and find the ASEDs to each fissure were about 1.8–2.8 mm (refer to Table 5). Due to this fact, we think, even in the cases of incomplete inter-lobe fissure on original CT images, our method could provide a reasonably approximate anatomical result of lung lobar identification (Fig. 11).

Table 5
The accuracy evaluations for the initial segmentation results of lung fissures (boundary of the lung lobes) using manual tracings

| 7 cases | ASED (mm) | | |
|---|---|---|---|
| | Right lung | | Left lung |
| | Oblique fissure | Horizontal fissure | Oblique fissure |
| Mean | 1.83 | 2.70 | 2.77 |
| S.D. | 0.76 | 3.04 | 1.01 |
| Maximum | 3.11 | 9.50 | 3.82 |
| Minimum | 1.15 | 1.24 | 1.35 |

### 4.6. Inter-lobe fissure extractions

Using the human tracings of inter-lobe fissures in the above section as a reference standard, we evaluated the accuracy of fissure extractions by our method for seven patient cases. We measured ASED from extracted fissures to the reference standard as the error of extraction. The ASED of each fissure, shown in Table 6, confirmed that our method can extract inter-lobe fissures precisely with an error of approximately 0.5 mm from the reference tracings. We confirmed that our method could identify inter-lobe fissures successfully from the CT images that have a normal lung structure and complete inter-lobe fissure as shown in Fig. 10. For cases in which the fissure is incomplete on CT images (Fig. 11), our method simply regarded the approximated lobar boundaries as the inter-lobe fissures and issued a warning of incompleteness.

The typical computation time of our scheme (Fig. 1) was about 105 min for one CT case using a computer (CPU: AMD Opteron (TM) Model 242), and the individual time for processing steps 1–5 in Fig. 1 was 11, 40, 4, 10, and 40 min, respectively. We are doing some works that can be expected to reduce the computation time using a PC cluster based on the message passing interface (MPI) library.

Lung region segmentation based on CT values of air used in this research was a well-known approach that has been reported in many research works [6,7]. The threshold value used in Ref. [6] was optimized by minimizing the variety of the mean density difference between air and human tissue regions after gray-level thresholding. This method has a similar effect to the [11] when the density distributions of air and body regions are not overlapped together. Lung contour smoothing has been introduced in some research works to close the lung hilum based on binary 2-D or 3-D morphology operations [18]. However, the binary morphology operation such as big ball rolling process always causes an excessive smoothing effect which deteriorates the extraction precision of lung surface. In order to solve this problem, a method was proposed to indicate the approximate range of lung hilum and close it using morphology operations [19]. However, this method needs the anatomical structure of airway tree to estimate the locations of lung hilums firstly. Our method (dividing lung surfaces, detecting the lung hilum locations, and

only smoothing the surface of lung hilum) can avoid accuracy deteriorations caused by smoothing the entire lung surface, and this process need not any other information for assistance except of lung surface itself [13]. The junction between left and right lungs after gray-level thresholding was also a problem in lung region segmentation. A popular solution was to separate left and right lungs and find the anterior and posterior junction using a binary morphological dilation [18]. Instead of binary morphological dilation, we used a 3-D watershed method to find the junction lines and separate the left and right lung regions based on gray-level information of lung regions. This method has been proved more accurate than the method based on binary morphological dilation.

The lung fissure identification and lobar extraction were reported in Refs. [20–26]. An approximation method to determine the lung segments based on the anatomical bronchial tree using CT images was proposed by Refs. [20,21]. However, due to the facts that the segmented bronchial tree (corresponding to the sixth- or seventh-order bronchi) cannot be recognized stably without any leak even based on high-resolution CT images, we found that the information of bronchial tree was not enough for automated lobe segmentation from CT images [22]. On the other hand, another approach to extract lung fissure and lobe using the lung vessels was proposed by Refs. [23,24]. This method was based on the hypothesis that the lung vessels do not exist around the lung fissures locations. However, this hypothesis was not always true in many cases; some improvements of this research works added the information of bronchial tree for fissure identification [25,26]. The basic idea of our method for lung fissure and lobe extraction was based on anatomical bronchial tree which was similar to Refs. [20,21], the difference was that we used the lung vessels running together with the each lobar bronchial tree to improve the accuracy of fissure location estimation and decided the lung fissures based on real gray-scale information [27]. Atlas-based fissure identification [28] may be a new direction for lung lobe segmentation using CT images, however, high-precision registration the of anatomical lung structure in CT images which is necessary not only for atlas generation but also for atlas-based segmentation had not be resolved completely till now.

The algorithms based on Hessian matrix analysis [29] proved very useful for vessel extraction. However, this algorithm needs a lot of the computation time. Our approach tries to extract the lung vessels roughly by a region growing algorithm and improve the accuracy by deleting the bronchial wall regions from it. This method did not cost a lot of computation time, however, depended on the accuracy of bronchial wall extractions.

## 5. Conclusion

We have developed a full-automatic classification scheme to recognize lung structures from high-resolution chest CT images. Our method divides the whole CT image into target organ and tissue regions sequentially, in a manner closely based on their anatomical relationships and statistical intensity distribution among different organ and tissue regions. The policy "region extraction → structure recognition → detail correction" is introduced as a basic rule of our processing flow, and the principal parameters of each process are self-optimized automatically and dynamically for purposes of adapting to different patient cases. We applied our method to high-resolution CT images from 44 patients and confirmed that our classification scheme could correctly and stably provide stratified recognition results of lung structures for 41 patients and failed in 3 patient cases (2 cases had serious pneumonias, 1 case had an abnormal tree structure of airway due to the serious pulmonary emphysema). The recognition results of this research provided the possibility to make a further analysis or visualization of vessel, bronchus and other abnormality such as pulmonary emphysema in a lobe-by-lobe base which is request by clinic medicine. In the future, we will attempt to classify the pulmonary vessels into artery and vein groups and recognize the anatomical structure of the mediastinum.

## Acknowledgements

The authors thank the members of Fujita's Laboratory and the Virtual System Laboratory (VSL) of Gifu University for their collaboration. This research was supported in part by research grants from the Collaborative Centre for Academy/Industry/Government and VSL of Gifu University, in part by the Ministry of Health, Labor, and Welfare under a Grant-In-Aid for Cancer Research, and in part by the Ministry of Education, Culture, Sports, Science and Technology under a Grant-In-Aid for Scientific Research from the Japanese Government.

## References

[1] http://www.gemedical.co.jp/rad/ct/lightspeed_ultral6_tech.html.
[2] http://www.toshiba-medical.co.jp/tmd/products/ct/aquilion/sixteen/index.html.
[3] Aykac D, Hoffman EA, Mclennan G, Reinhardt JM. Segmentation and analysis of the human airway tree from three-dimensional X-ray CT images. IEEE Trans Med Imag 2003;22(8):940–50.
[4] Mori K, Hasegawa J, Suenaga Y, Toriwaki J. Automated anatomical labeling of the bronchial branch and its application to the virtual bronchoscopy system. IEEE Trans Med Imag 2000;19(2):103–14.
[5] Mori K, Hasegawa J, Toriwaki J, Anno H, Katada K. Automated extraction of bronchus area from three dimensional X-ray CT images. IEICE Tech Rep 1994;142.
[6] Hu S, Hoffman EA, Reinhardt JM. Automatic lung segmentation for accurate quantitation of volumetric X-ray CT images. IEEE Trans Med Imag 2001;20(6):490–8.
[7] Leader JK, Zheng B, Rogers RM, Sciurba FC, Perez A, Chapman BE, et al. Automated lung segmentation in X-ray computed tomography. Acad Radiol 2003;10(11):1224–36.
[8] Kitasaka T, Mori K, Hasegawa J, Toriwaki J. Automated extraction of the lung area from 3-D chest X-ray CT images based upon the 3-D shape model deformation. In: Proceedings of the 13th International congress and exhibition on computer aided radiology and surgery. 1999. p. 194–8.
[9] Kitasaka T, Mori K, Hasegawa J, Toriwaki J, Katada K. A method for automated extraction of aorta and pulmonary artery using line models from 3-D chest X-ray CT images with contrast medium. In: Proceedings of 16th conference on pattern recognition. 2002. p. III-273–6.
[10] http://medical.nema.org/.
[11] Otsu N. A threshold selection method from gray-level histogram. IEEE Trans SMC 1979;SMC-9(1):62–6.
[12] Sekiguchi H, Sugimoto N, Eiho S, Hanakawa T, Urayama S. A blood vessel segmentation for head MRA using branch-based region-growing. IEICE Trans Info Sys DII 2004;J87(1):126–33.

[13] Murata N, Zhou X, Hara T, Fujita H, Yokoyama R, Kiryu T, et al. Automated extraction of hilus pulmonis from multi-slice chest CT image, IEICE Tech Rep MI2002-101; 2002. p. 31–5 [in Japanese].
[14] Medlar EM. Variations in interlobar fissure. AJR 1947;57:723–5.
[15] Raasch BN, Carsky EW, Lane EJ, O'Callaghan JP, Heitzman ER. Radiographic anatomy of the interlobar fissure: a study of 100 specimens. AJR 1982;138:1043–9.
[16] Saito T, Toriwaki J. Euclidean distance transformation for three dimensional digital images. Trans IEICE 1993;J76-D-II(3):445–53 [in Japanese].
[17] Zhou X, Hara T, Fujita H, Ida Y, Katada K, Matsumoto K. Extraction and recognition of the thoracic organs based on 3-D CT images and its application. In: Proceedings of the 16th international congress and exhibition of computer assisted radiology and surgery 2002. 2002. p. 776–81.
[18] Brown MS, McNitt-Gray MF, Mankovich NJ, Goldin JG, Hiller J, Wilson LS, et al. Method for segmenting chest CT image data using an anatomical model: preliminary results. IEEE Trans Med Imag 1997;16:828–39.
[19] Ukil S, Reinhardt JM. Smoothing lung segmentation surface in 3D X-ray CT images using anatomical guidance. Proc SPIE Med Imag 2004 2004;5370:1066–75.
[20] Krass S, Selle D, Boehm D, Jend H-H, Kriete A, Rau W, et al. A method for the determination of bronchopulmonary segments based on HRCT data. In: Proceedings of the 14th international congress and exhibition of computer assisted radiology and surgery, 2000. 2000. p. 584–9.
[21] http://www.mevis.de/.
[22] Hayashi T, Zhou X, Hara T, Fujita H, Yokoyama R, Kiryu T, et al. Classification of lung lobes based on bronchus from chest multi-slice CT images. Trans IEICE 2003;J87-D-II(1):134–45 [in Japanese].
[23] Mukaibo T, Kawata Y, Niki N, Ohmatsu H, Kakinuma R, Kanekp M, et al. Classification of lung area using multidetector-row CT images. Proc SPIE Med Imag 2002 2002;3(22):1292–300.
[24] Kuhnigk J, Hahn HK, Hindennach M, Dicken V, Krass S, Peitgen H. Lung lobe segmentation by anatomy-guided 3D watershed transform. Proc SPIE Med Imag 2003 2003;5032:1482–90.
[25] Saita S, Kubo M, Kawata Y, Niki N, Ohmatsu H, Moriyama N. An extraction algorithm of pulmonary fissures from low-dose multi-slice CT image. Trans IEICE 2003;J87-D-II(1):357–60 [in Japanese].
[26] Saita S, Yasutomo M, Kubo M, Kawata Y, Niki N, Eguchi K, et al. An extraction algorithm of pulmonary fissures from multi-slice CT image. Proc SPIE Med Imag 2004 2004;5370:1590–7.
[27] Zhou X, Hayashi T, Hara T, Fujita H, Yokoyama R, Kiryu T, et al. Automatic recognition of lung lobes and fissures from multislice CT images. Proc SPIE Med Imag 2004 2004;5370:1629–33.
[28] Zhang L, Hoffman EA, Reinhardt JM. Atlas-driven lung lobe segmentation in volumetric X-ray CT images. Proc SPIE Med Imag 2003 2003;5031:308–19.
[29] Sato Y, Nakajima S, Shiraga N, Atsumi H, Yoshida S, Koller T, et al. Three-dimensional multi-scale line filter for segmentation and visualization of curvilinear structures in medical images. Med Image Anal 1998;2(2):143–68.

**Xiangrong Zhou** received the MS and PhD degree in information engineering from Nagoya University, Japan in 1997 and 2000, respectively. From 2000 to 2002, he continued his research in medical image processing as a postdoctoral researcher at Gifu University, and currently, he is an instructor of Graduate School of Medicine, Gifu University, Japan. His research interests include medical image analysis, medical image visualization and pattern recognition.

**Tatsuro Hayashi** received the BS degree in Department of Information Science, Faculty of Engineering in 2003 and MS degree in Department of Intelligent Image Information Graduate School of Medicine in 2005 from Gifu University. Currently, he is a PhD candidate in Graduate School of Medicine of Gifu University, Japan. His research interests include medical image processing and computer-aided diagnosis.

**Takeshi Hara** received the MS and PhD degrees in electrical engineering from Gifu University, Japan, in 1994 and 2000, respectively. He is currently an associate professor in the Department of Intelligent Image Information, Graduate School of Medicine, Gifu University, Japan. His research interests include computer network, medical image processing and pattern recognition.

**Hiroshi Fujita** received the BS and MS degrees in electrical engineering from Gifu University, Japan, in 1976 and 1978, respectively, and PhD degree from Nagoya University in 1983. He was a research associate at University of Chicago, USA, from 1983 to 1986. He is currently a Chairman and a professor in the Department of Intelligent Image Information, Graduate School of Medicine, Gifu University, Japan. His research interests include computer-aided diagnosis system, image analysis and processing, and image evaluation in medicine.

**Ryujiro Yokoyama** received the BS and MS degree in electrical engineering from Gifu University, Japan, in 2000 and 2002, respectively. Currently, he is a PhD candidate in Graduate School of Medicine from Gifu University, Japan. He is also a radiological technologist and working in Gifu University Hospital from 1976 till now. His research interests include medical image processing and pattern recognition.

**Takuji Kiryu** received the PhD degree at Gifu University in 2001. He served as a visiting fellow at Department of Radiology, Armed Forced Institute of Pathology (AFIP) in 2003. He has been appointed to the assistant professor of Department of Radiology at Gifu University School of Medicine since 2001.

**Hiroaki Hoshi** received the PhD degree at Miyazaki Medical School in 1987. He served as a visiting scholar at the Montreal Neurological Institute from 1991 to 1992. He has been appointed to the Chairmanship of Department of Radiology at Gifu University School of Medicine since 1995.